Journal of Cluster Science (2020) 31:601–607
https://doi.org/10.1007/s10876-019-01698-2

BRIEF COMMUNICATION

Structural and Electronic Properties of Nano-brass: Cu_xZn_y ($x + y = 11 - 13$) Clusters

Qiman Liu[1] · Chang Xu[1] · Longjiu Cheng[1,2]

Received: 20 September 2019 / Published online: 10 October 2019

Abstract

Cu–Zn brasses are one kind of the typical Hume-Rothery alloys, of which the phase stability mechanisms are decided by the electronic effects. Cu–Zn clusters can be considered as a sort of alloys with a particle size at nanometer scale. The structures of small-sized Cu–Zn clusters have been well established up to 10 atoms, but the structural evolution behavior of larger clusters is still not well-known. In this work, the geometric structures of Cu_xZn_y clusters in a size range ($x + y = 11 - 13$) are investigated by using a method combining the genetic algorithm with density functional theory. A series of relevant structures of the clusters are obtained, and the structural evolution diagrams are plotted depending on the relative energy. It was found that the Cu–Zn clusters with even number of valence electrons (n^*) exhibit high stability. When $n^* = 12$ and 14, the clusters adopt prolate motifs, which have similar electronic structures to O_2 and F_2 molecules, respectively, based on the super valence bond model. When $n^* = 18$ and 20, the clusters keep spherical cage motifs, which satisfy the magic numbers of Jellium model and could be viewed as stable superatoms.

Keywords Alloy cluster · Structural prediction · Superatom · Chemical bonding

Introduction

Metallic clusters have attracted much attention due to their large range of unusual physicochemical properties and many promising applications [1–7]. The study of clusters represents one of the fields of greatest growth in nanostructured materials science. Particularly, the development of superatom clusters consisting of metal atoms that mimic the chemical behavior of elements has been explored extensively in recent years [8–16]. They can be used not only as building blocks for assembling materials but also as new functional materials themselves by manipulation of their composition, shape, and size [17, 18]. In general, superatoms are typified by complete geometric and electronic shell closings [19]. The electronic shells in superatoms are expressed by superatomic orbitals, named 1S, 1P, 1D, 2S, 1F, 2P, and so on in order of orbital energy. Thus, the electron counts that achieve a particularly stable configuration are 2, 8, 18, 20, 34, 40, 58, and 92… This theory of superatom has achieved great success in explaining the stability of spherical metal clusters [20–26].

However, clusters are not always spherical. In 2003, Cheng et al. developed the super valence bond (SVB) model [27, 28], which gives one more generalized insight into the electronic structures of superatomic clusters. In this model, a prolate cluster is divided into two spherical blocks sharing nucleus and valence pairs at the border to achieve electronic closed shell. This bonding pattern between superatoms is defined as the SVB which has the similar characteristics as the bonding pattern between simple atoms [29–34]. Taking the prolate Li_{10} cluster as an example [27], it could be viewed as the union of two 7c-5e (seven-center five-electron) spherical superatoms sharing a four-nucleus tetrahedron and three covalent pairs, which is the analogues of F_2 in bonding framework.

Cu–Zn alloys have a variety of crystal structures. Earlier studies revealed that the structures of Cu–Zn alloys correlate with the average number of valence electrons or the

✉ Longjiu Cheng
clj@ustc.edu

[1] Department of Chemistry, Anhui University, Hefei 230601, Anhui, People's Republic of China

[2] Anhui Province Key Laboratory of Chemistry for Inorganic/Organic Hybrid Functionalized Materials, Hefei 230601, Anhui, People's Republic of China

electron-per-atom (e/a) ratio [35–40]. Cu–Zn clusters can be considered as a sort of alloys with a particle size at nanometer scale. Very recently, we found that, just as in bulk brass, the structures of Cu_xZn_y clusters in a size range ($x + y = 3 - 10$) are determined by the total number of valence electrons (n^*), where the clusters with same n^* have similar geometric motifs [41]. Due to the complexity of potential energy surfaces, especially for large size clusters, the global minimum search is specially challenging. Botticelli et al. have studied 13-atom Cu–Zn clusters [42], and the results indicate that the Cu-rich clusters tend to have compact geometries, often icosahedral, such as Cu_6Zn_7 and Cu_8Zn_5. However, the electronic structures of the clusters were not analyzed.

Hence, we started our explorations of the size-dependent growth behavior of the Cu_xZn_y ($x + y = 11 - 13$) clusters related to their geometric and electronic properties. To gain the most reliable structures of Cu–Zn systems, the potential energy surfaces of the clusters are scanned by using genetic algorithm (GA) [43, 44] with density functional theory (DFT). Our results show great diversity and flexibility in geometric and electronic structures for the Cu–Zn clusters. The electronic stability and chemical bonding patterns are also discussed.

Computational Methods

The geometries of Cu_xZn_y ($x + y = 11 - 13$) clusters are located by unbiased global search of the DFT potential energy surface with GA directly using the BP86-D3 functional [45] that was proven to give reasonably accurate energetic properties of the small Cu–Zn clusters [41]. At the global optimization procedure, a small basis set (def2-SVP) and a loose convergence criterion are adopted for saving calculation time. After global optimization, the low-lying candidates are fully relaxed at the BP86-D3/def2-TZVP [46]. Energies of the structures reported herein include the contribution of zero point energy (ZPE) corrections. All first principle calculations in this work are carried out on the GAUSSIAN 09 package [47], and molecular visualization is performed using MOLEKEL 5.4 software [48].

Results and Discussion

Using the combination of GA and DFT, we obtained a series of relevant structures for Cu_xZn_y ($x + y = 11 - 13$) clusters at the BP86-D3/def2-TZVP level. The vibrational frequencies are checked to ensure that the structures are true local minima at the same theoretical level.

Geometric Structures and Structural Evolution Diagrams

To give a direct view of the structural evolution of the Cu–Zn binary systems, the structural evolution diagrams (SEDs) are plotted in Fig. 1, presenting information of stability *versus* composition. To give a reasonable measure of stability of the Cu_xZn_y clusters, the relative energy (E_{rel}) is calculated by taking Cu_2 molecule and Zn atom as references:

$$E_{rel} = xE(Cu_2)/2 + yE(Zn) - E(Cu_xZn_y),$$

wherein $E(Cu_xZn_y)$, $E(Cu_2)$ and $E(Zn)$ are energies of Cu_xZn_y, Cu_2 molecule and Zn atom, respectively. E_{rel} is a key indicator for stability of a Cu–Zn cluster, and is useful to compare the relative stability of Cu–Zn clusters at different compositions. Here we take Cu_2 molecule as the reference instead of Cu atom, because Cu atom has half-filled $4s^1$ orbital and usually has higher binding energy than Zn atoms ($4s^2$). Hence base lines of the curves of E_{rel} are obliquely upward with number of Cu atoms. To further evaluate the relative stability of these clusters, the curves of E_{rel} are fitted by the form $E_{ave} = a + bx$ as the base lines. It is seen that the peaks of E_{rel} correspond to particularly stable structures and are labeled by green circles in the figure. The global minimum (GM) structures are also labeled in the SEDs.

Figure 1a plots the SED of the 11-atom clusters. Zn_{11} with D_{3h} symmetry can be obtained by two Zn atoms capped on tricapped trigonal prism (TTP) Zn_9 [49]. The structure of Cu_1Zn_{10} with C_{4v} symmetry is built from Cu_1Zn_9 cage by adding one Zn atom, connected to Cu. Cu_2Zn_9 is in C_s symmetry. Cu_3Zn_8, Cu_4Zn_7 and Cu_5Zn_6 adopt similar motifs, which are spherical cages. For Cu_6Zn_5 and Cu_7Zn_4, the structures are based on body-fused bi-octahedron. Cu_8Zn_3, Cu_9Zn_2, $Cu_{10}Zn_1$ and Cu_{11} have similar prolate structures.

Figure 1b plots the SED of the 12-atom clusters. Zn_{12} can be seen as the distorted Zn_9 plus three-capped Zn atoms. The structure of Cu_1Zn_{11} with C_s symmetry is built from the Cu_1Zn_9 with Zn_2 linked to the cage. The structure of Cu_2Zn_{10} is based on the Cu_2Zn_9, while Cu_3Zn_9 is based on the Cu_3Zn_8. Cu_4Zn_8 is in C_s symmetry. Cu_5Zn_7, Cu_6Zn_6 and Cu_7Zn_5 are icosahedral cages. Cu_8Zn_4, Cu_9Zn_3, $Cu_{10}Zn_2$, $Cu_{11}Zn_1$ and Cu_{12} are prolate structures.

Figure 1c plots the SED of the 13-atom clusters. Zn_{13} can be seen as the distorted Zn_9 plus four-capped Zn atoms. Cu_1Zn_{12} with C_s symmetry is a distorted pillar structure. The structural frameworks of Cu_2Zn_{11} and Cu_3Zn_{10} are based on the Cu_2Zn_9 and Cu_4Zn_7, respectively. Cu_4Zn_9 is in C_{2v} symmetry. Cu_5Zn_8, Cu_6Zn_7 and Cu_7Zn_6 are icosahedral cages linked to one separate Zn atom. Cu_8Zn_5 and

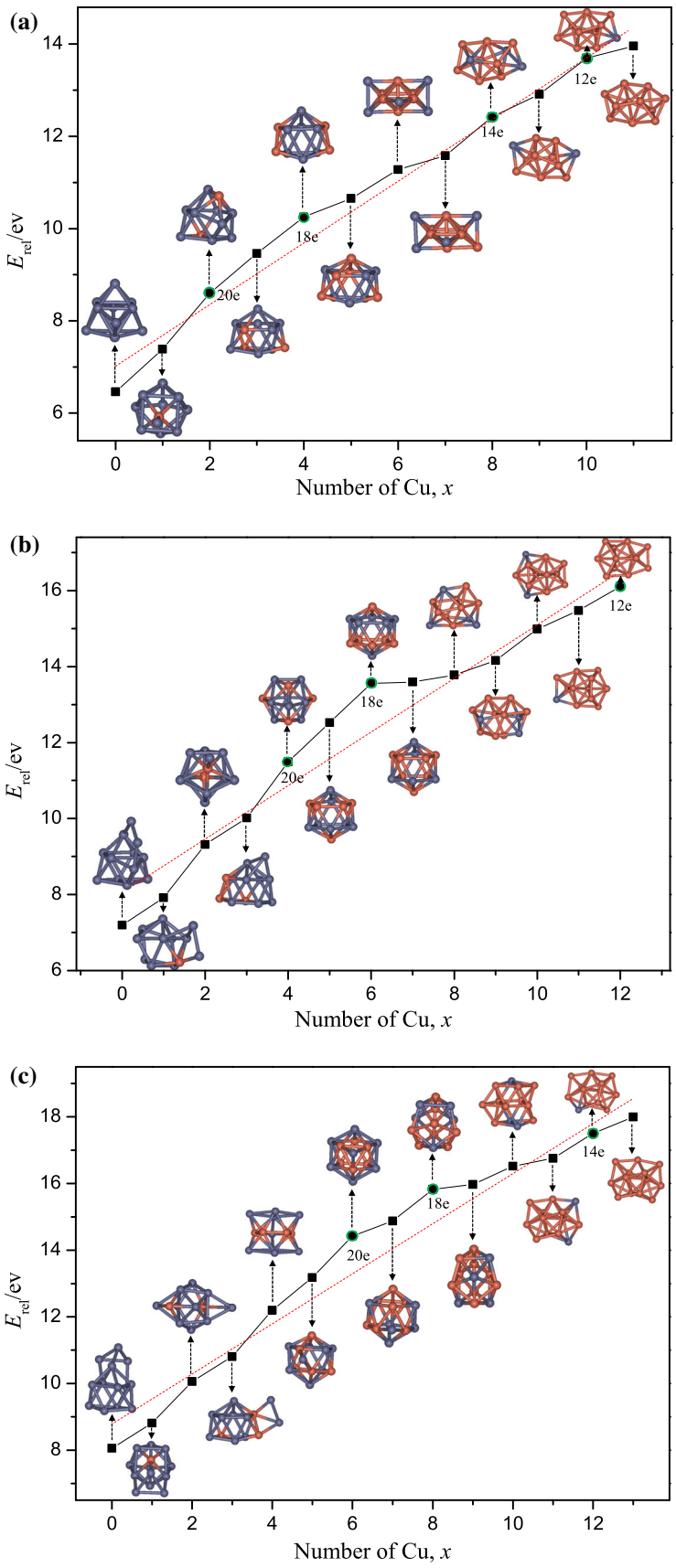

Fig. 1 Structural evolution diagrams (SEDs) of **a** $x + y = 11$, **b** $x + y = 12$ and **c** $x + y = 13$ of Cu_xZn_y clusters. The curves of E_{rel} are fitted by the form $E_{ave} = a + bx$ as the base lines which are represented by red dash lines. Cu-brown; Zn-gray

Cu_9Zn_4 adopt similar motifs. $Cu_{11}Zn_2$, $Cu_{12}Zn_1$ and Cu_{13} are prolate structures.

However, geometry optimizations at the PBE/LANL2DZ level reveal that the most stable structures of Cu_6Zn_7 and Cu_8Zn_5 clusters are icosahedra [42]. Figure 2 displays the newly located GM and low-energy isomers of Cu_6Zn_7 and Cu_8Zn_5 at the BP86-D3/def2-TZVP level. The symmetry point groups and relative energies of the clusters are also given. It can be seen that the structures of these isomers are in accord with the rule formulated by Teo et al. [50]. Moreover, isomers 6-7A and 8-5A are more stable than icosahedral 6-7E and 8-5H by 0.23 eV and 0.37 eV, respectively. To further verify the reliability of different functionals of DFT methods, a benchmark calculation is carried out by comparing the relative stability of five isomers of Cu_8Zn_5 cluster. Table 1 gives the results of the benchmark calculation at the DFT and CCSD(T) levels with the def2-TZVP basis set. 8–5(I–IV) are four cage structures, and 8-5 V is an icosahedral structure. Note that BP86, BP86-D3, PBE, PBE0, and PW91 functionals are consistent with CCSD(T) method in the energetic sequences of the four cage isomers. However, the relative stability of the icosahedral 8-5 V is highly overestimated by DFT functionals except M062x and TPSS. The comparison suggests that BP86-D3/def2-TZVP method is reliable in predicting relative stability of Cu_8Zn_5 cluster.

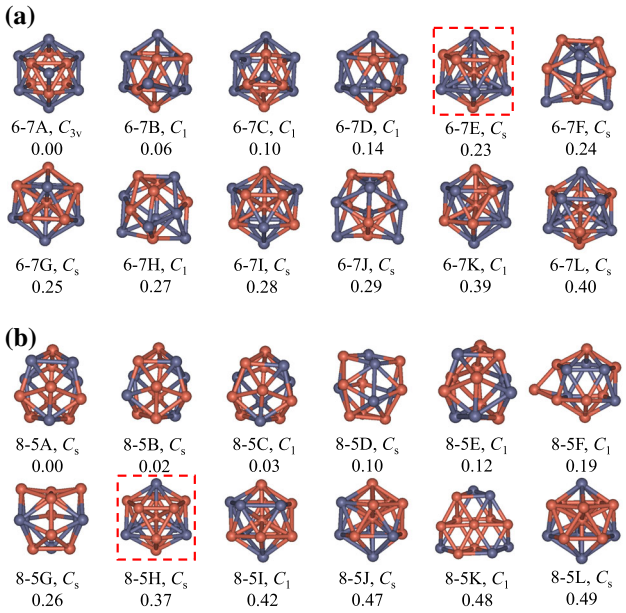

Fig. 2 Optimized structures and relative stability of **a** Cu_6Zn_7 and **b** Cu_8Zn_5 at BP86-D3/def2-TZVP level. Labeled are symmetry and energy (eV) relative to the global minimum one. Cu-brown; Zn-gray

Table 1 Cu_8Zn_5 isomer relative energies at the CCSD(T) and DFT levels with the def2-TZVP basis set

Method	8-5I	8-5II	8-5III	8-5IV	8-5 V
CCSD(T)	0.00	0.08	0.22	0.23	0.08
BP86	0.00	0.08	0.20	0.26	0.57
BP86-D3	0.00	0.10	0.19	0.26	0.37
PBE	0.00	0.10	0.20	0.26	0.37
PBE-D3	0.00	0.11	0.20	0.26	0.28
PBE0	0.00	0.09	0.24	0.27	0.40
PBE0-D3	0.00	0.10	0.24	0.28	0.32
B3LYP	0.00	0.03	0.25	0.25	0.94
B3LYP-D3	0.00	0.05	0.24	0.25	0.72
TPSSh	0.00	0.14	0.20	0.25	0.03
TPSS	0.03	0.19	0.21	0.28	0.00
TPSS-D3	0.14	0.31	0.32	0.39	0.00
M06	0.00	0.07	0.28	0.24	0.60
M062x	0.00	0.13	0.34	0.24	0.10
PW91	0.00	0.10	0.20	0.26	0.46
Ref*	0.06	0.11	0.34	0.25	0.00

*Energies are calculated at the PBE/LANL2DZ level from Ref. [42]

Electronic Structures

As shown in the SEDs, Cu–Zn clusters with certain n^* number (as labeled by green circles in the SEDs) exhibit high stability. In order to reach understanding of this phenomenon, we focus on the electronic characteristics and bonding features of these clusters.

As shown in Fig. 3, the 12e ($Cu_{10}Zn_1$ and Cu_{12}) and 14e (Cu_8Zn_3 and $Cu_{12}Zn_1$) are prolate clusters. Based on the SVB model of superatomic molecules, a prolate cluster can be seen as an integration of two spherical superatoms sharing atomic nuclei and valence electrons. To give a straight forward view on the chemical bonding of these clusters, we employ the adaptive natural density partitioning (AdNDP) method as a tool for analysis [51–53]. The AdNDP is a generalized natural bonding orbital (NBO) search method to discuss the localized and delocalized multicenter bonds (coded as nc-2e, that is, an n-center two-electron bond). Figure 3a plots the structures and chemical bonding patterns of the 12e clusters. AdNDP analysis reveals that $Cu_{10}Zn_1$ has four super lone pairs (LPs) with occupancy number ON = 1.85–1.96 |e|, one 11c-2e super σ-bond (ON = 2.00 |e|), and one 11c-2e super π-bond (ON = 2.00 |e|), which resembles the singlet O_2 molecule in bonding framework. The situation in Cu_{12} cluster is also similar.

Figure 3b plots the structures and chemical bonding patterns of the 14e clusters. AdNDP analysis shows that, the 14 electrons of Cu_8Zn_3 are delocalized in two

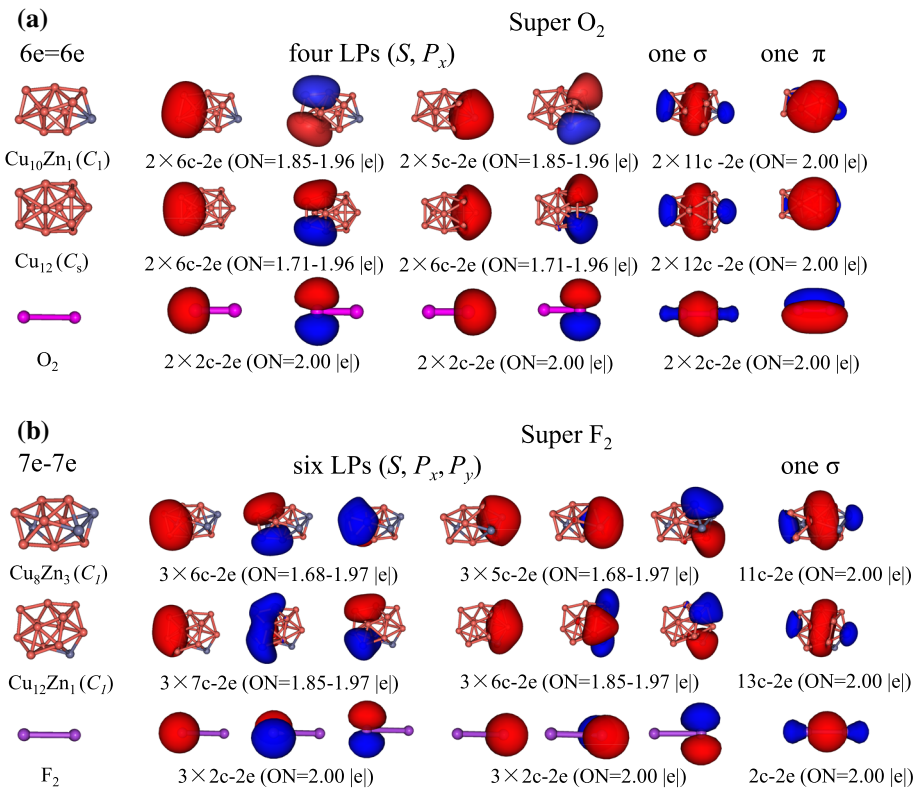

Fig. 3 Structures and AdNDP localized natural bonding orbitals of **a**: the 12e ($Cu_{10}Zn$, Cu_{12} and O_2) clusters and **b**: the 14e (Cu_8Zn_3, $Cu_{12}Zn_1$, and F_2) clusters

superatoms, including two S-type super LPs, four P-type super LPs, and one super σ-bond. Thus, Cu_8Zn_3 is an analogue of F_2 molecule. Similar bonding feature has also been identified in $Cu_{12}Zn_1$ cluster.

The 18e (Cu_4Zn_7, Cu_6Zn_6 and Cu_8Zn_5) are spherical clusters which are in geometric shell closure. Based on the Jellium model, a metal cluster can be considered as a superatom since valence electrons confined in a jellium-like potential field are accommodated in a series of quantized orbitals. Figure 4 plots structures and the molecular orbital (MO) diagrams of the three clusters. For the 18e compounds, the lowest MO has 1S character, and the next three MOs exhibit dominant 1P character, then followed by five nearly degenerate 1D orbitals. Thus, electronic shells of the 18e compounds are $(1S)^2(1P)^6(1D)^{10}$.

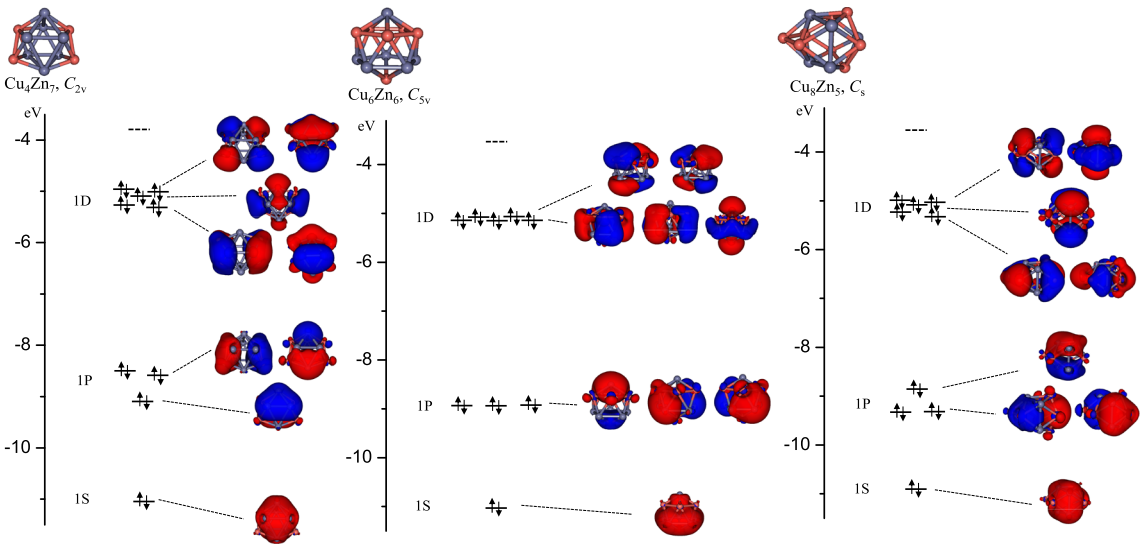

Fig. 4 Structures and the MO diagrams of the 18e (Cu_4Zn_7, Cu_6Zn_6 and Cu_8Zn_5) clusters

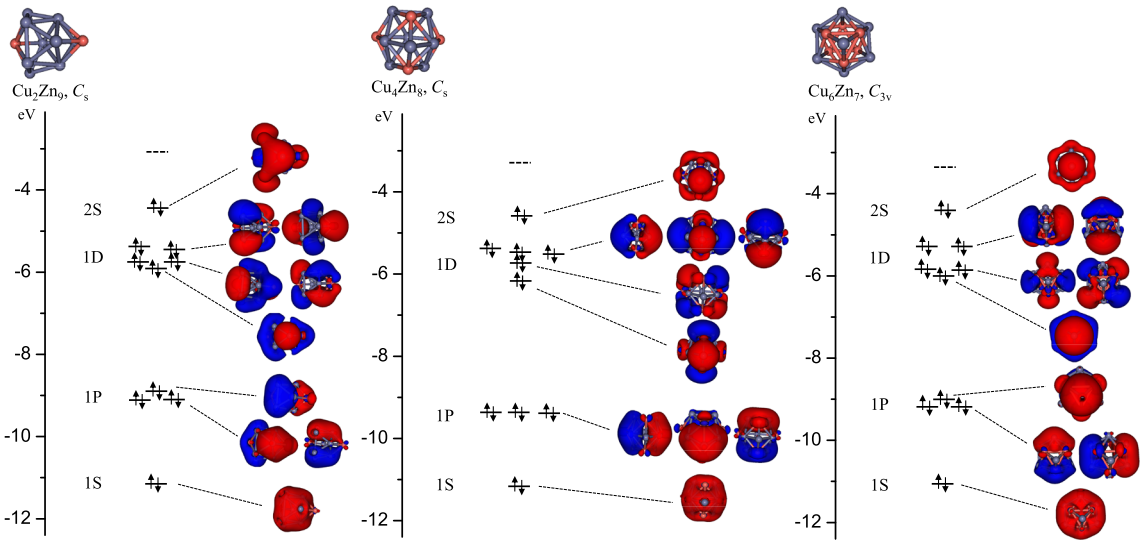

Fig. 5 Structures and the MO diagrams of the 20e (Cu_2Zn_9, Cu_4Zn_8 and Cu_6Zn_7) clusters

Figure 5 plots structures and the MOs of the 20e (Cu_2Zn_9, Cu_4Zn_8 and Cu_6Zn_7). It can be seen that the 20 valence electrons of the clusters are distributed on superatomic shells resembling atomic orbitals involving 1S orbital, three 1P orbitals, five 1D orbitals and 2S orbital. Thus, electronic shells of the 20e compounds are $(1S)^2(1P)^6(1D)^{10}(2S)^2$. Each cluster has completely filled shells, which is consistent with the magic species of Jellium model.

Conclusions

In summary, the geometric and electronic structures and chemical bonding of a series of Cu_xZn_y clusters in the size range $(x + y = 11 - 13)$ were investigated by using the GA-DFT method. Benchmark calculations indicate that the method (BP86-D3/Def2-TZVP) used in this work is reliable in predicting the energetic sequences of different isomers of Cu_8Zn_5 clusters compared to CCSD(T) method. The SEDs that depend on the relative energy were given to investigate structural evolution of the clusters. It was found that the Cu–Zn clusters with even valence electron numbers exhibit high stability. The 12e ($Cu_{10}Zn_1$ and Cu_{12}) and 14e (Cu_8Zn_3 and $Cu_{12}Zn_1$) have prolate structures, which resemble O_2 and F_2 molecule in bonding frameworks, respectively. The 18e (Cu_4Zn_7, Cu_6Zn_6 and Cu_8Zn_5) and 20e (Cu_2Zn_9, Cu_4Zn_8 and Cu_6Zn_7) adopt spherical cage motifs, where each cluster satisfies the magic number of Jellium model and could be viewed as a stable superatom.

Acknowledgements This work is financed by the National Natural Science Foundation of China (21873001), and by the Foundation of Distinguished Young Scientists of Anhui Province. The calculations were carried out at the High-Performance Computing Center of Anhui University.

References

1. R. Ferrando, J. Jellinek, and R. L. Johnston (2008). *Chem. Rev.* **108**, 845–910.
2. H.-L. Liu, F. Nosheen, and X. Wang (2015). *Chem. Soc. Rev.* **44**, 3056–3078.
3. H. Zhang, T. Watanabe, M. Okumura, M. Haruta, and N. Toshima (2011). *Nat. Mater.* **11**, 49.
4. M. Sankar, Q. He, M. Morad, J. Pritchard, S. J. Freakley, J. K. Edwards, S. H. Taylor, D. J. Morgan, A. F. Carley, D. W. Knight, C. J. Kiely, and G. J. Hutchings (2012). *ACS Nano* **6**, 6600–6613.
5. S. Pande, T. Jian, N. S. Khetrapal, L.-S. Wang, and X. C. Zeng (2018). *J. Phys. Chem. C* **122**, 6947–6954.
6. I. Demiroglu, K. Yao, H. A. Hussein, and R. L. Johnston (2017). *J. Phys. Chem. C* **121**, 10773–10780.
7. W. Benten, N. Nilius, N. Ernst, and H. J. Freund (2005). *Phys. Rev. B* **72**, 045403.
8. Z. Luo and A. W. Castleman (2014). *Acc. Chem. Res.* **47**, 2931–2940.
9. W. D. Knight, K. Clemenger, W. A. de Heer, W. A. Saunders, M. Y. Chou, and M. L. Cohen (1984). *Phys. Rev. Lett.* **52**, 2141–2143.
10. K. Clemenger (1985). *Phys. Rev. B* **32**, 1359–1362.
11. W. A. de Heer (1993). *Rev. Mod. Phys.* **65**, 611–676.
12. P. Pyykkö and N. Runeberg (2002). *Angew. Chem. Int. Ed.* **41**, 2174–2176.
13. P. Jena (2013). *J. Phys. Chem. Lett.* **4**, 1432–1442.
14. A. Muñoz-Castro (2013). *J. Phys. Chem. Lett.* **4**, 3363–3366.
15. V. Chauhan, A. C. Reber, and S. N. Khanna (2018). *Nat. Commun.* **9**, 2357.
16. J. P. Mojica-Sánchez, R. Flores-Moreno, K. Pineda-Urbina, and Z. Gómez-Sandoval (2018). *ACS Omega* **3**, 11252–11261.
17. S. N. Khanna and P. Jena (1992). *Phys. Rev. Lett.* **69**, 1664–1667.
18. P. Jena and Q. Sun (2018). *Chem. Rev.* **118**, 5755–5870.
19. A. C. Reber and S. N. Khanna (2017). *Acc. Chem. Res.* **50**, 255–263.

20. A. W. Castleman and S. N. Khanna (2009). *J. Phys. Chem. C* **113**, 2664–2675.
21. D. E. Bergeron, P. J. Roach, A. W. Castleman, N. O. Jones, and S. N. Khanna (2005). *Science* **307**, 231–235.
22. H. Häkkinen (2008). *Chem. Soc. Rev.* **37**, 1847–1859.
23. D.-E. Jiang and S. Dai (2009). *Inorg. Chem.* **48**, 2720–2722.
24. M. Zhang, J. Zhang, X. Feng, H. Zhang, L. Zhao, Y. Luo, and W. Cao (2013). *J. Phys. Chem. A* **117**, 13025–13036.
25. X. Zhang, Y. Wang, H. Wang, A. Lim, G. Gantefoer, K. H. Bowen, J. U. Reveles, and S. N. Khanna (2013). *J. Am. Chem. Soc.* **135**, 4856–4861.
26. K. Koyasu and T. Tsukuda (2014). *Phys. Chem. Chem. Phys.* **16**, 21717–21720.
27. L. Cheng and J. Yang (2013). *J. Chem. Phys.* **138**, 141101.
28. L. Cheng, Y. Yuan, X. Zhang, and J. Yang (2013). *Angew. Chem. Int. Ed.* **52**, 9035–9039.
29. L. Cheng, X. Zhang, B. Jin, and J. Yang (2014). *Nanoscale* **6**, 12440–12444.
30. Z. Tian and L. Cheng (2015). *Phys. Chem. Chem. Phys.* **17**, 13421–13428.
31. L. Yan, L. Cheng, and J. Yang (2015). *J. Phys. Chem. C* **119**, 23274–23278.
32. L. Liu, P. Li, L.-F. Yuan, L. Cheng, and J. Yang (2016). *Nanoscale* **8**, 12787–12792.
33. H. Wang and L. Cheng (2017). *Nanoscale* **9**, 13209–13213.
34. Q. Zheng, C. Xu, X. Wu, and L. Cheng (2018). *ACS Omega* **3**, 14423–14430.
35. V. J. Keast, J. Ewald, K. S. B. De Silva, M. B. Cortie, B. Monnier, D. Cuskelly, and E. H. Kisi (2015). *J. Alloys Compd.* **647**, 129–135.
36. K. Freitag, H. Banh, C. Gemel, R. W. Seidel, S. Kahlal, J.-Y. Saillard, and R. A. Fischer (2014). *Chem. Commun.* **50**, 8681–8684.
37. K. Freitag, C. Gemel, P. Jerabek, I. M. Oppel, R. W. Seidel, G. Frenking, H. Banh, K. Dilchert, and R. A. Fischer (2015). *Angew. Chem. Int. Ed.* **127**, 4445–4449.
38. R. S. Dhaka, S. Banik, A. K. Shukla, V. Vyas, A. Chakrabarti, S. R. Barman, B. L. Ahuja, and B. K. Sharma (2008). *Phys. Rev. B* **78**, 073107.
39. A. A. Pankova, V. A. Blatov, G. D. Ilyushin, and D. M. Proserpio (2013). *Inorg. Chem.* **52**, 13094–13107.
40. J. Hambrock, M. K. Schröter, A. Birkner, C. Wöll, and R. A. Fischer (2003). *Chem. Mater.* **15**, 4217–4222.
41. Q. Liu and L. Cheng (2019). *J. Alloys Compd.* **771**, (2019), 762–768.
42. J. Botticelli, R. Fournier, and M. Zhang (2008). *Theor. Chem. Acc.* **120**, 583–589.
43. R. L. Johnston (2003). *Dalton Trans.* **22**, 4193–4207.
44. Z. Tian and L. Cheng (2017). *J. Phys. Chem. C* **121**, 20458–20467.
45. J. P. Perdew (1986). *Phys. Rev. B* **33**, 8822–8824.
46. F. Weigend and R. Ahlrichs (2005). *Phys. Chem. Chem. Phys.* **7**, 3297–3305.
47. G.W.T. M. J. Frisch and H. B. Schlegel et al., GAUSSIAN 09, Revision, G. B. 01, Inc., Wallingford, CT, 2009.
48. U.M. Varetto, version 5.4. 0.8; Swiss National, S. Supercomputing Centre: Manno, 2009.
49. J. Wang, G. Wang, and J. Zhao (2003). *Phys. Rev. A* **68**, 013201.
50. B. K. Teo and A. Strizhev (2002). *Inorg. Chem.* **41**, 6332–6342.
51. D. Y. Zubarev and A. I. Boldyrev (2008). *Phys. Chem. Chem. Phys.* **10**, 5207–5217.
52. D. Y. Zubarev and A. I. Boldyrev (2008). *J. Org. Chem.* **73**, 9251–9258.
53. W. Huang, A. P. Sergeeva, H.-J. Zhai, B. B. Averkiev, L.-S. Wang, and A. I. Boldyrev (2010). *Nat. Chem.* **2**, 202.